Journal of Molecular Structure 1282 (2023) 135213

Contents lists available at ScienceDirect

Journal of Molecular Structure

journal homepage: www.elsevier.com/locate/molstr

New oxadiazole/triazole derivatives with antimicrobial and antioxidant properties

Sam Dawbaa[a,b,c,*], Demokrat Nuha[a,d,e], Asaf Evrim Evren[a,f], Meral Yilmaz Cankiliç[g], Leyla Yurttaş[a], Gülhan Turan[a]

[a] Anadolu University, Faculty of Pharmacy, Department of Pharmaceutical Chemistry, 26470, Eskişehir, Turkey
[b] Thamar University, Faculty of Medical Sciences, Department of Doctor of Pharmacy (PharmD), Dhamar, Yemen
[c] Al-Hikma University, Faculty of Medical Sciences, Department of Pharmacy, Dhamar, Yemen
[d] Eskisehir Technical University, Faculty of Science, Department of Chemistry, 26555, Eskişehir, Turkey
[e] University of Business and Technology, Faculty of Pharmacy, Prishtina, Kosovo
[f] Bilecik Şeyh Edebali University, Vocational School of Health Services, Department of Pharmacy Services, Bilecik, Turkey
[g] Eskisehir Technical University, Faculty of Science, Department of Biology, 26555, Eskişehir, Turkey

ARTICLE INFO

Article history:
Received 22 November 2022
Revised 2 January 2023
Accepted 20 February 2023
Available online 21 February 2023

Keywords:
Oxadiazole
Triazole
Antimicrobial activity
Antioxidant
Molecular dynamics simulation

ABSTRACT

In the search for new antimicrobial agents, we synthesized a new series of oxadiazole and triazole derivatives. The series of *N*-(benzothiazol-2-yl)-2-{{5-[(2-chlorophenoxy)methyl]-1,3,4-oxadiazol-2-yl}thio}acetamide (**4a-4e**) and *N*-(benzothiazol-2-yl)-2-{{5-[(2-chlorophenoxy)methyl]-4-(4-chlorophenyl)-4H-1,2,4-triazol-3-yl}thio}acetamide (**7a-7e**) derivatized at the C6 of benzothiazole ring were synthesized and tested for their antimicrobial and antioxidant activity. The compounds were analyzed via ^{1}H NMR, ^{13}C NMR, and HRMS. The pharmacokinetic profile of the targeted compounds was predicted via *in silico* calculations. None of the tested compounds showed promising antibacterial or antifungal activity in comparison to the used reference agents. Compounds **4a** and **7a** showed some antioxidant potency in comparison to ascorbic acid but their activity did not match exactly that of ascorbic acid. The binding modes for compounds **4a** and **7a** were revealed and the optimum poses of the compounds in the active site of the tested oxidant enzyme peroxiredoxin 5 (PRDX5) were displayed via a molecular docking study. Molecular dynamics simulation studies for compound **7a** showed the key amino acids in the active site of the enzyme and gave information regarding the mechanism of enzyme interaction. DFT calculations were also made for compounds **4a** and **7a**.

1. Introduction

Antimicrobial resistance (AMR) is a major issue today [1]. The roots of this issue are the inactivation of antibiotics, target mutation caused by foreign genes, activation of efflux pump, enhancement of bacterial virulence, or formation of biofilm [2–7]. These mechanisms render available medicines (monotherapies and combination therapies [8–11]) ineffective. Hence, researchers now aim to block the development of AMRs [12,13], find new treatment paradigms [14,15], or develop entirely new agents with superior activity [16–19]. Although all these purposes are very valuable, a few decades later, current drugs may not be used clinically because of AMR as foreseen by various reports [20,21]. Even if the treatment strategy is usually effective nowadays whilst applying combo chemotherapeutics (β-lactamase inhibitor+β-lactam antibiotic), according to the above reports, new compounds are needed desperately. Currently used some antifungal agents are shown in Fig. 1.

In the latter direction, compounds that contain an oxadiazole or triazole ring have been intensely studied. In addition to being exceptional antimicrobials, these compounds display significant antioxidant properties [22–24]. This idiosyncratic feature enables oxadiazole- and triazole-based compounds to address bacterial inflammation and combat resistant bacterial types [25]. Moreover, they can act on peroxiredoxins (Prxs), a family of enzymes that play a critical role in immune responses following microbial infection [26]. For these reasons, designing and biochemically assessing new oxadiazole- and/or triazole-based compounds could lead to a powerful new class of antimicrobial agents.

Toward the development of next-generation oxadiazole- and triazole-based antimicrobials, our group designed and tested a novel set of compounds. Our scaffolds not only feature the oxa-

* Corresponding author at: Department of Doctor of Pharmacy (PharmD), Faculty of Medical Sciences, Thamar University, Dhamar, Yemen.
E-mail addresses: sdawbaa@tu.edu.ye, dawbaa655@anadolu.edu.tr (S. Dawbaa).

https://doi.org/10.1016/j.molstruc.2023.135213
0022-2860/

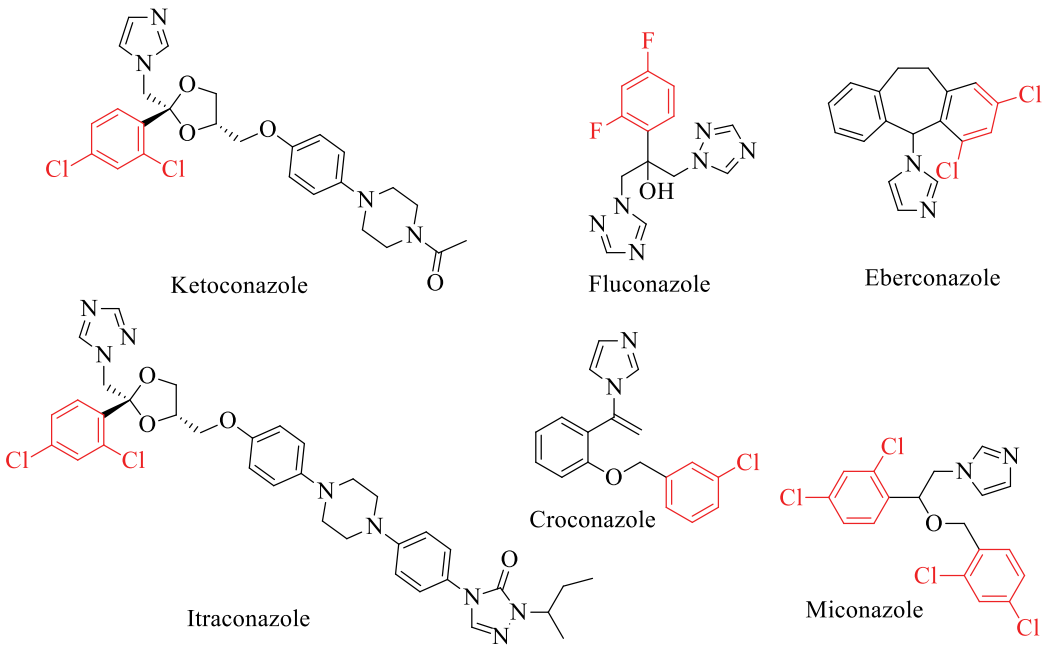

Fig. 1. Antifungal agents including halogen-substituted phenyl rings.

diazole or triazole ring but incorporate other functional groups known to impart significant antimicrobial and/or antioxidant activity. These include (1) benzothiazole ring [27–30], (2) ether or thioether linkage [31–35], (3) aromatic hydroxyl group, and (4) halogenated arene [36,37], We now report the original synthesis and preliminary testing (in vitro and *in silico* studies) of our newly conceived compounds.

2. RESULTS and discussion

2.1. Chemistry

In this study, ten new compounds were synthesized which included the *N*-(benzothiazol-2-yl)−2-{{5-[(2-chlorophenoxy)methyl]−1,3,4-oxadiazol-2-yl}thio}acetamide (**4a–4e**) and *N*-(benzothiazol-2-yl)−2-({5-[(2-chlorophenoxy)methyl]−4-(4-chlorophenyl)−4*H*-1,2,4-triazol-3-yl}thio)acetamide (**7a–7e**) nuclei in their structures. The synthesis is illustrated in Scheme 1. Initially, the ethyl 2-(2-chlorophenoxy)acetate (**1**) was catenated from 2-chlorophenol and ethyl 2-chloroacetate [38]. Then, the obtained compound **1** was treated with hydrazine monohydrate to gain 2-(2-chlorophenoxy)acetohydrazide (**2**). Next, compound **2** was treated with potassium hydroxide and carbon disulfide to synthesize 5-((2-chlorophenoxy)methyl)−1,3,4-oxadiazole-2-thiol (**3**) [38]. Compound **3** was then reacted with *N*-(benzothiazol-2-yl)−2-chloroacetamide derivatives to gain the respective *N*-(benzothiazol-2-yl)−2-({5-[(2-chlorophenoxy)methyl]−1,3,4-oxadiazol-2-yl}thio)acetamide derivatives (**4a–4e**). On the other hand, 2-[2-(2-chlorophenoxy)acetyl]-*N*-(4-chlorophenyl)hydrazinecarbothioamide (**5**) were catenated from 2-(2-chlorophenoxy)acetohydrazide (**2**) and 1−chloro-4-isothiocyanatobenzene. To synthesize 5-[(2-chlorophenoxy)methyl]−4-(4-chlorophenyl)−4*H*-1,2,4-triazole-3-thiol (**6**), compound **5** was treated with potassium hydroxide under reflux. Finally, compound **6** was reacted with *N*-(benzothiazol-2-yl)−2-chloroacetamide derivatives in acetone to obtain their respective *N*-(benzothiazol-2-yl)−2-({5-[(2-chlorophenoxy)methyl]−4-(4-chlorophenyl)−4*H*-1,2,4-triazol-3-yl}thio)acetamide derivatives (**7a–7e**) as core structure. The structures of the synthesized compounds (**4a–4e**) and (**7a–7e**) were confirmed by proton and ^{13}C nuclear magnetic resonance (^{1}H NMR and ^{13}C NMR), and high-resolution mass spectroscopy (HRMS).

2.2. Pharmacokinetic parameters

The computational results are shown in Table 1. Seven compounds were in line with Lipinski's RoF [39] (The footnote of Table 1 displays the desired value for each parameter). According to Lipinski, any compound is expected to be orally bioavailable if it does not violate at all or violates at most only one rule of the RoF. Hence, compounds **7b, 7d,** and **7e** are predicted to show problematic drug-like characters because they violated more than one rule of the RoF. The water solubility of the synthesized compounds is generally poor. The higher the Log S value the better the solubility in water. On the other hand, the lipophilicity of compounds **4a-4e** complies with the required prerequisites of the lipophilicity of drugs. However, the partitioning of compounds **7a-7e** between octanol and water was predicted to be poor and out of the acceptable range for a compound to have a good lipophilicity characteristic of a standard drug. The polarity of the compounds can still affect oral bioavailability and permeation through the blood-brain barrier (BBB). The polarity descriptor TPSA was calculated and predicted to negatively affect the absorption of most of the compounds from the gastrointestinal tract (GIT). As a result, the absorption from the GIT and permeation through BBB is expected to be poor for all of the compounds due to the effect of at least two of the above-described physicochemical descriptors (Log S, Log $P_{o/w}$, and TPSA).

The skin permeability of the target compounds in this study was predicted by calculating its descriptor Log K_p. All of the compounds are thought that they will have good penetration inside the dermal layers. Thus, this will make the topical route of administration to the skin a better candidate than the systemic route. From another point of view, these compounds are expected to be administrable topically elsewhere like to the eye and mouth safely. This expectation was concluded from the poor BBB permeability and low GI absorbability of the compounds.

In conclusion, the topical application of the synthesized compounds to the skin, eyes, ears, or mouth is considered the best route of administration if the compounds proved a useful thera-

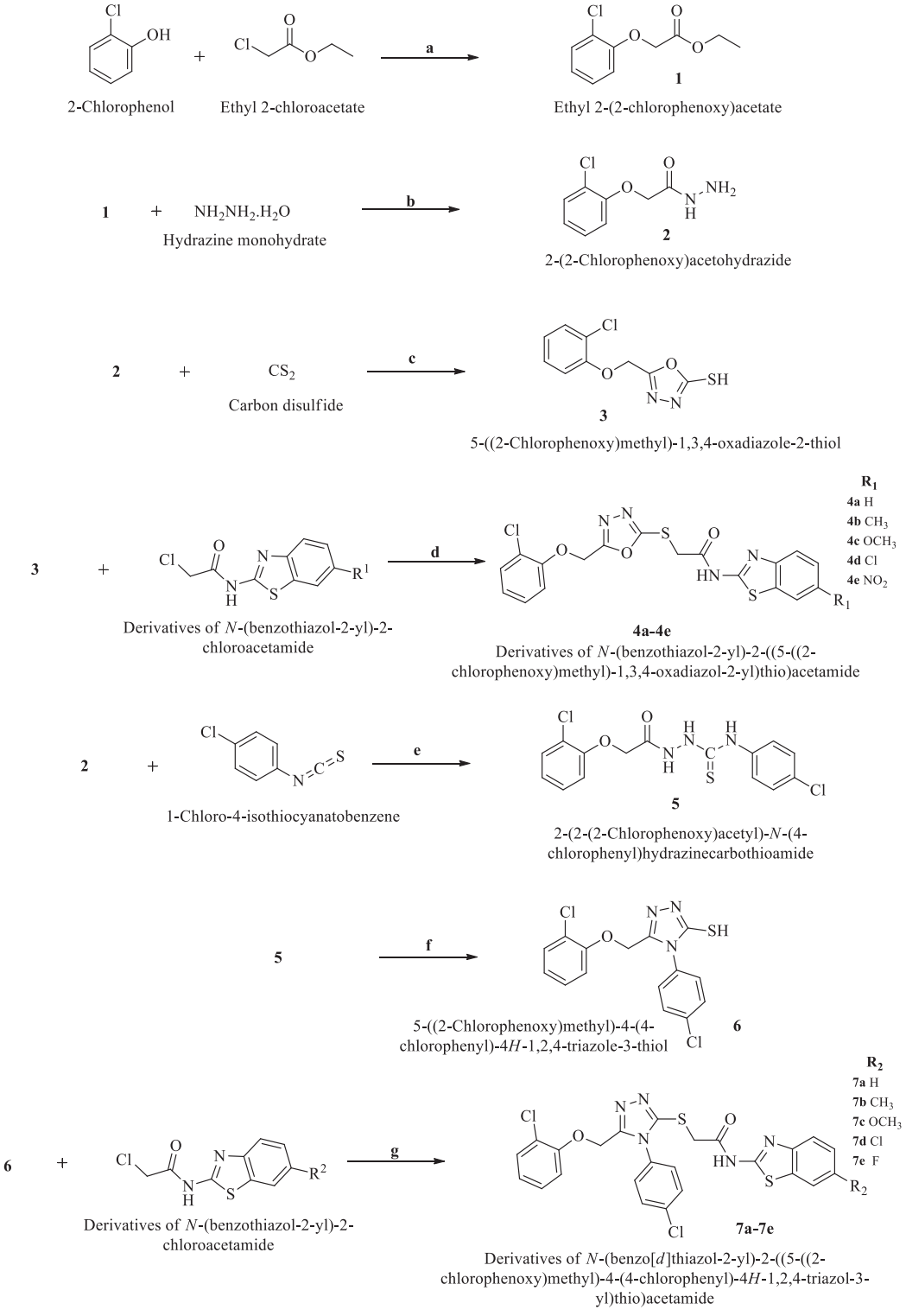

Scheme 1. The synthesis diagram of the compounds 4a-4e and 7a-7e. Reagents and conditions: (a) Acetone, K_2CO_3, reflux, 24 h; (b) EtOH, 0–5 °C, then RT, 3 h; (c) KOH, EtOH, reflux, 5 h; (d) Acetone, K_2CO_3, RT, overnight; (e) EtOH, reflux, 3 h; (f) 2 M KOH, EtOH, reflux, 4 h; (g) Acetone, RT, 5 h.

peutic efficacy of any kind. Additionally, the low GI absorbability of the compounds reduces any potential systemic toxicity and potentiates the idea of their use topically in the treatment of GI infections when topical activity is required in some conditions like some fungal infections.

2.3. Biology

2.3.1. Antimicrobial activity

The antimicrobial activity of the final ten compounds (**4a-4e** and **7a-7e**) was tested on various gram-positive, and gram-negative

Table 1
Physicochemical, pharmacokinetic, and medicinal chemistry properties of the final compounds (by SwissAdme) (4a–4e) and (7a–7e).

	Physicochemical Properties					Pharmacokinetics		Medicinal Chemistry	
	HBA	HBD	TPSA	Log Po/w	Log S	GIA	Log Kp	RoF (V)	SA
4a	6	1	143.68	3.72	−7.16	Low	−5.80	Yes (0)	3.39
4b	6	1	143.68	4.06	−7.53	Low	−5.63	Yes (0)	3.45
4c	7	1	152.91	3.72	−7.32	Low	−6.01	Yes (0)	3.58
4d	6	1	143.68	4.22	−7.81	Low	−5.57	Yes (0)	3.46
4e	8	1	189.50	2.91	−7.94	Low	−6.20	Yes (0)	3.57
7a	5	1	135.47	5.24	−9.02	Low	−5.08	Yes (1)	3.61
7b	5	1	135.47	5.56	−9.39	Low	−4.91	No (2)	3.71
7c	6	1	144.70	5.19	−9.18	Low	−5.28	Yes (1)	3.81
7d	5	1	135.47	5.73	−9.67	Low	−4.84	No (2)	3.68
7e	6	1	135.47	5.53	−9.12	Low	−5.12	No (2)	3.66
RF- 1	9	6	181.62	−0.40	−3.64	Low	−8.83	Yes (1)	5.17
RF- 2	7	1	81.65	0.88	−1.63	High	−7.92	Yes (0)	2.91

HBA: H-bond acceptor (≤10), **HBD:** H-bond donor (≤5), **TPSA:** Topologic polar surface area (≤140 Å²) **Log Po/w** (−0.7 to 5), **Log S:** Water Solubility (−6.5 to 5), **GIA:** Gastrointestinal absorption, **Log Kp:** skin permeation (between −8 and −1 cm/s) **RoF (V):** Rule of Five (violation number, 0 or 1 is acceptable), **SA:** Synthetic accessibility from 1 (very easy) to 10 (very difficult). **RF- 1:** Tetracycline, **RF-2:** Fluconazole.

Table 2
MIC values of the compounds (μg/mL).

	4a	4b	4c	4d	4e	7a	7b	7c	7d	7e	SD-1	SD-2
A	–	–	–	–	500	–	500	–	–	500	62.50	nt
B	–	–	–	–	–	–	62.50	–	–	125	31.25	nt
C	500	500	500	500	250	500	–	125	500	500	15.63	nt
D	–	–	–	–	–	–	–	–	–	500	125	nt
E	–	–	–	–	–	–	–	–	–	–	31.25	nt
F	–	–	–	–	–	–	–	–	–	–	125	nt
G	250	250	250	–	500	500	500	500	500	500	nt	62.50
H	250	250	250	–	500	–	–	–	500	500	nt	31.25
I	250	250	250	–	500	500	500	500	500	500	nt	62.50
J	–	–	–	–	–	–	–	–	–	–	nt	62.50
K	500	500	250	250	500	250	250	500	250	250	nt	62.50
L	500	–	500	500	500	500	–	500	500	–	nt	62.50
M	500	–	250	500	500	–	–	500	250	–	nt	62.50
N	500	500	500	500	500	500	–	500	500	–	nt	31.25
O	250	–	250	500	500	500	500	500	250	–	nt	62.50

- No activity, **nt:** Not tested, **SD-1:** Chloramphenicol, **SD-2:** Ketoconazole. **A:** *Bacillus cereus* ATCC 10876; **B:** *Bacillus subtilis* NRRL NRS-744; **C:** *Micrococcus luteus* NRRL B-4375; **D:** *Staphylococcus aureus* ATCC 6538; **E:** *Escherichia coli* ATCC 25922; **F:** *Salmonella thyphimurium* ATCC 14028; **G**: *Candida albicans* ATCC 90028; **H:** *Candida krusei* ATCC 6258; **I:** *Candida parapsilopsis* ATCC 22019; **J:** *Candida glabrata* ATCC 90030; **K:** *Aspergillus niger* ATCC 6275; **L:** *Aspergillus flavus* ATCC 9807 **M:** *Aspergillus fumigatus* NRRL 113; **N:** *Penicillium notatum* (clinical isolate); **O:** *Penicillium chryrsogenum* ATCC 10106.

bacteria, yeasts, and filamentous fungi (Table 2). Among gram-positive bacteria, our compounds showed no significant activity against *B. cereus, S. aureus,* and *M. luteus*. Some compounds showed no activity at the highest tested concentration on the aforementioned microorganisms. Compound **7b** showed half the antimicrobial potential of the standard drug, chloramphenicol, on *B. subtilis* which is another gram-positive bacterium. None of the compounds exhibited activity on gram-negative bacteria *E. coli* and *S. thyphimurium*. When the antifungal effects of the compounds on *Candida* species were evaluated, it was understood that oxadiazole derivatives were more active than triazole derivatives with half MIC values of them, mostly. But this potential is not as much as the standard drug, ketoconazole. None of the compounds showed activity against *C. glabrata*. When the activity against molds was evaluated, *A. flavus* appears to be the most resistant of the three *Aspergillus* strains tested. It has been determined that the MIC values of the compounds were 500 μg/mL and above. In addition, compounds **4c, 4d, 7a, 7b, 7d,** and **7e** showed inhibition against *A. niger* at 250 μg/mL concentration, while compounds **4c** and **7d** showed similar potential against *A. fumigatus*. The MIC value of the standard drug ketoconazole against these molds was found to be 62.50 μg/mL. The compounds showed greater activity against *P. chrysogenum* of the two tested *Penicillium* species than *P. notatum*, but this ratio did not approach the MIC value of the standard ketoconazole.

Table 3
Antioxidant activity of the compounds.

Compounds	IC_{50} (mg/mL)
4a	2.75
4b	4.11
4c	9.41
4d	8.67
4e	4.71
7a	2.67
7b	9.08
7c	5.04
7d	5.60
7e	18.07
Ascorbic acid	0.49

2.3.2. Antioxidant activity

The antioxidant activity of the substances was measured by applying the 1,1-diphenyl-2-picryl-hydrazyl (DPPH) method, and the free radical scavenger of the extract solutions was indicated as% inhibition of DPPH absorption. The DPPH scavenging effect (% inhibition) was calculated according to Eq. (1). The results in Table 3 showed the DPPH scavenging ability (IC_{50}) of tested concentrations of the substances at 520 nm by UV–visible spectrophotometer. Considering the IC_{50} values, it was concluded that the antioxidant activities of the substances were lower than ascorbic acid. The substance with the highest antioxidant activity was compound **7a**,

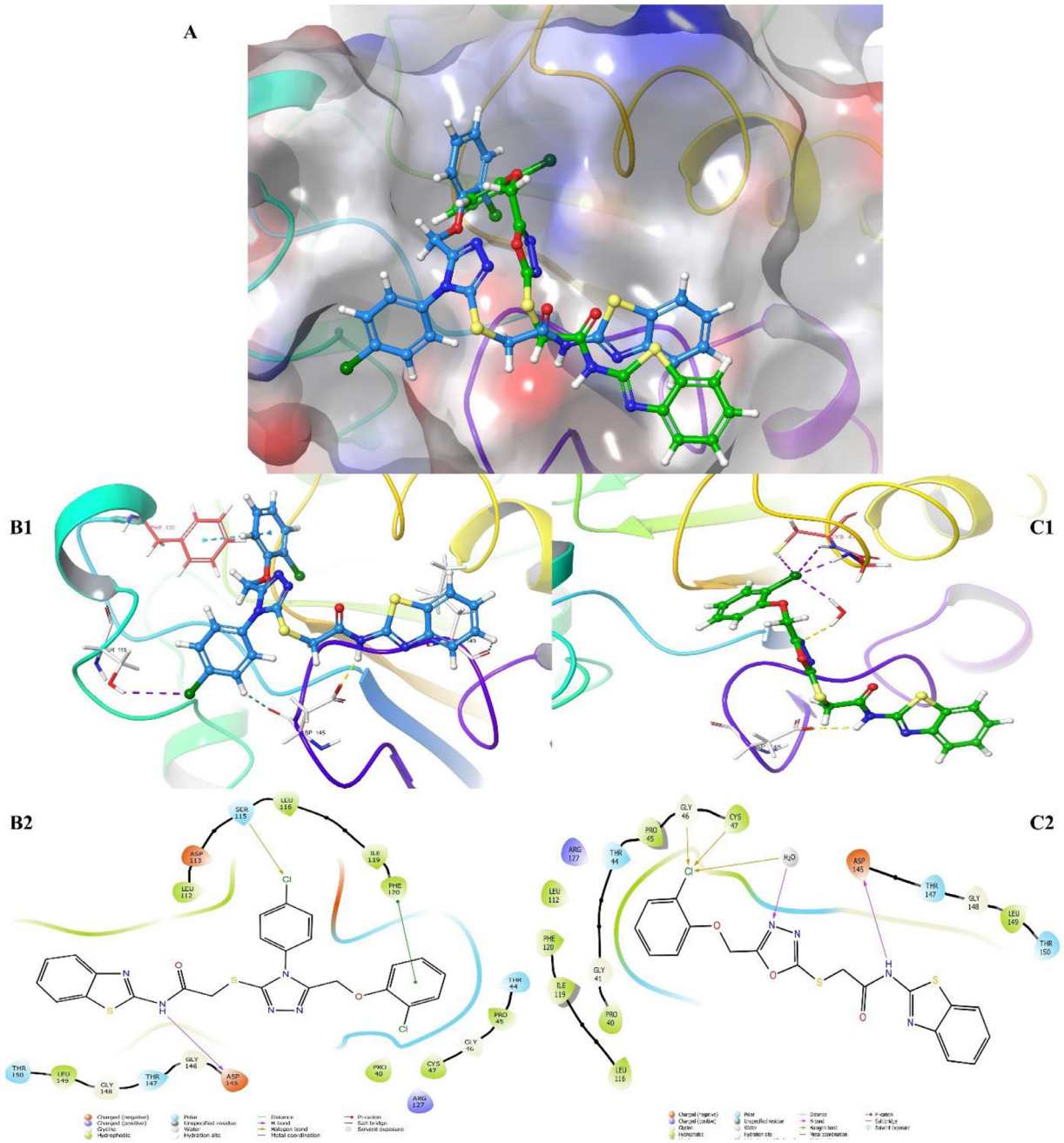

Fig. 2. The docking poses of the active compounds. A: Superimposition of compound 4a (green carbons) and compound 7a (blue carbons) inside the active pocket of the PRDX5 enzyme. B1 and B2: 3D and 2D pose of compound 7a at the active pocket. C1 and C2: 3D and 2D poses of compound 4a.

and the lowest was compound **7e**. The activity of the other samples was listed as **4a, 4b, 4e, 7c, 7d, 7b,** and **4c** in descending order.

2.4. In silico studies

2.4.1. Docking study on peroxiredoxin 5 enzyme (PRDX5)

Understanding and explaining the SAR at the molecular level aids rational drug design. According to the experimental antioxidant activity results, compounds **4a** and **7a** are more potent than the other compounds, but unfortunately not as effective as ascorbic acid. Here, we focused on clarifying the SAR and designing new molecules based on these compounds. Hence, further *in silico* studies were performed for this purpose.

According to docking results, both compounds localize in the reduced peroxiredoxin 5 active regions. It's clearly said that 2-chlorophenyl and benzothiazole moieties of both compounds land at the same part of the protein according to the 3D pose (Fig. 2-**A**). Also, the common interaction between the enzyme and the ligands was seen as an H-bond with Asp145 amino acid. This interaction is between amidic nitrogen (as an H-bond donor) and carboxylic acid oxygen (as an H-bond acceptor) of Asp145. Moreover, this residue is described as unique for PRDX5, thus, it has an impact on the selectivity of the PRDX5 enzyme [40]. Although there were not any in vitro tests on peroxiredoxin enzymes (hORF6: human PRDX6; and HBP23: rat PRDX1), this interaction pointed out this situation, which was also supported by the literature [41]. On the other hand, compound **4a** bonded to the enzyme via two direct halogen bonds,

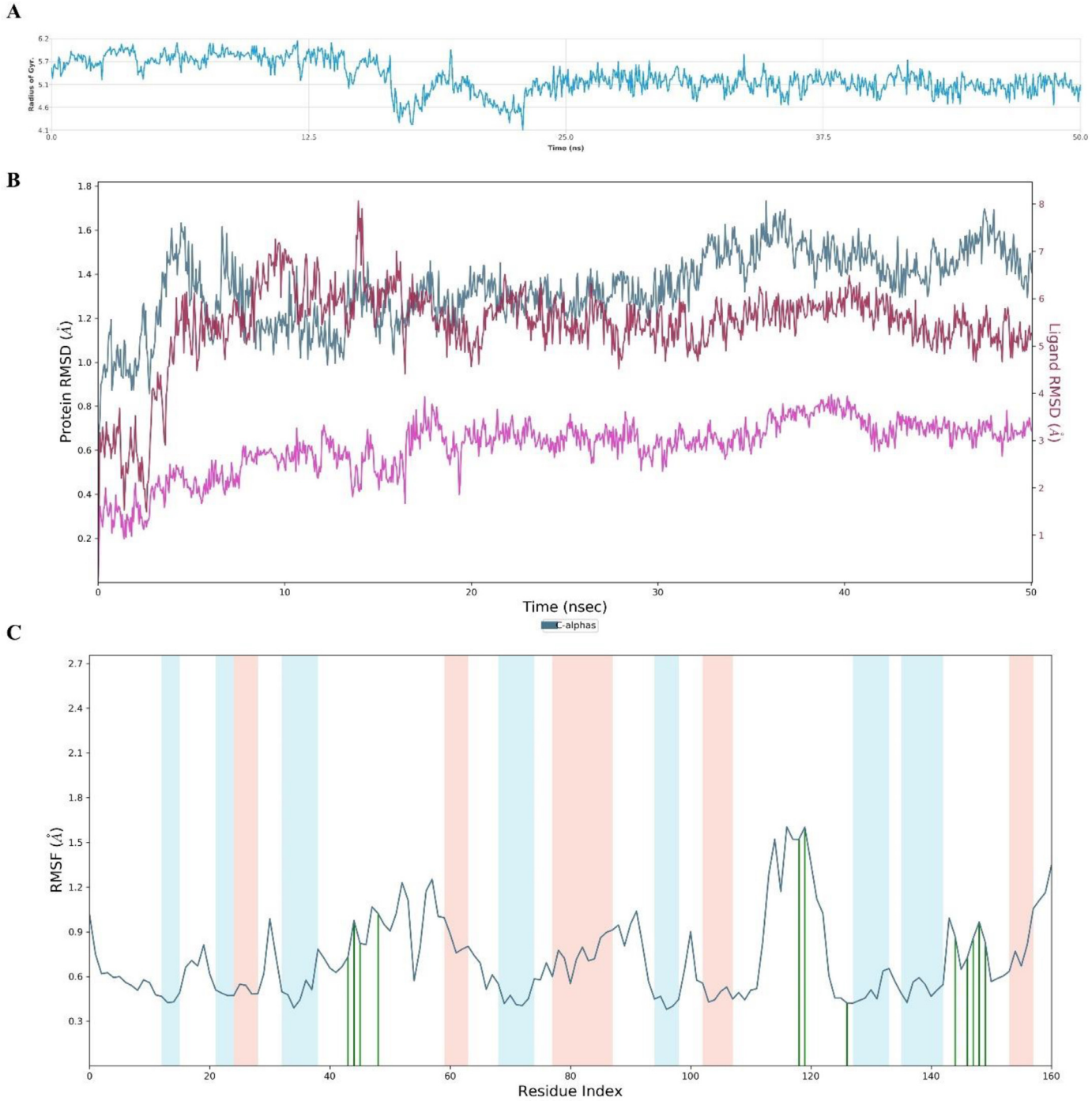

Fig. 3. The stability diagrams of the compound 7a-PRDX5 enzyme complex. A: Radius of gyration diagram; B: RMSD plot of ligand and protein during the simulation; C: RMSF plot of amino acids.

besides H-bond with Arg145. These interactions were made with Gly46 and Cys47, and these are described as the key amino acids of the enzyme-mediated antioxidant activity. Furthermore, one water-mediated halogen bond was formed intramolecularly between one of the oxadiazole nitrogen atoms and a chlorine atom. This interaction increased the activity by increasing the stability of the ligand-enzyme complex.

Regarding compound **7a**, several interactions with the enzyme were formed including one halogen bond with Ser115, one aromatic H-bond with Arg145, and one π-π stacking with Phe120, and H-bond with Arg145. Although compound **7a** showed a docking pose in the enzyme similar to that of **4a**, there was no observable interaction with Cys47 amino acid. Since the difference was the absence of interaction with Cys47 loop amino acid, an advanced investigation was planned to clarify its binding mode interaction with the enzyme. Hence, the interaction of compound **7a** with the PRDX5 enzyme was investigated against time using the molecular dynamics simulation (MDS) technique.

2.4.2. Molecular dynamics simulation study of 7a-PRDX5 complex

In the MDS study, the stability indicators are the Rg (Radius of gyration) plot, RMSD (Root mean square deviation) plot, and RMSF (root mean square fluctuations) plot (Fig. 3), and in this study, they

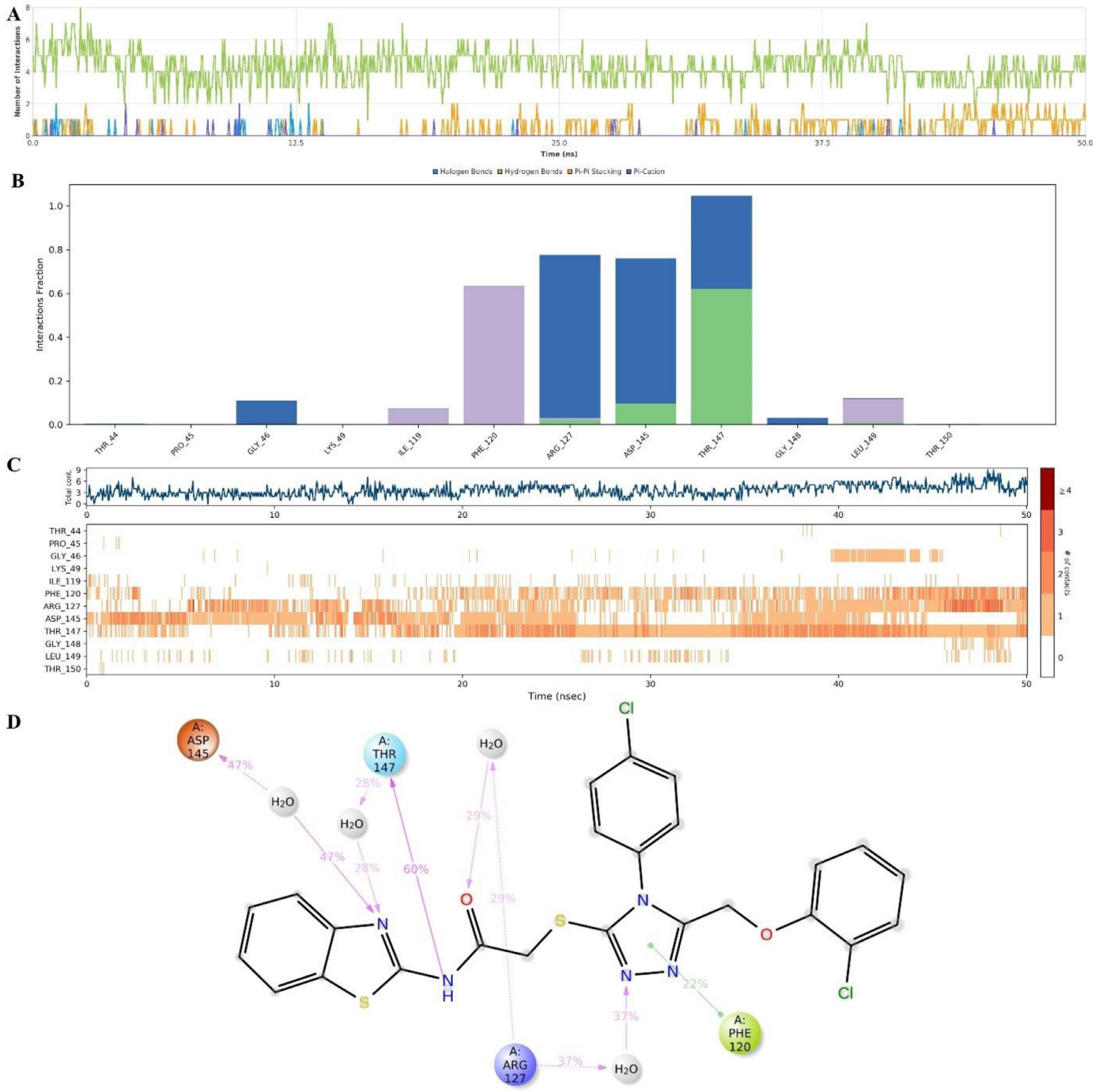

Fig. 4. The interaction diagrams of the compound 7a-PRDX5 enzyme complex. A: Number of interactions-interaction types-time plot; B: Interaction fraction-residue diagram; C: Total connections-residues-time plot; D: 2D interaction pose with connection strength (cut off=0.2) at the active region.

all pointed out that the stability of the complex is preserved during the simulation. However, the fluctuations were observed between 16.45–23.00 ns in the Rg plot. Therefore, it can be concluded that the stability is protected except in that time range. On the other hand, the RMSD plot also confirmed protecting the stability of the system during the entire simulation time. As a result, the stability was protected after 23.00 ns, and never cut off. The indicated instability between 16.45–23.00 ns probably originated from the movement of the protein, then its movement also affected the ligand, even so, the complex reached the system stability.

According to MDS results, compound **7a** formed H-bonds with Arg127, Asp145, and Thr147. Moreover, it also bonded to Gly46, Arg127, Asp145, Thr147, and Gly148 via a water-mediated H-bond. Additionally, it was observed that three hydrophobic interactions between **7a** and the residues Ile119, Phe120, and Leu149. Additionally, compound **7a** formed aromatic H-bonds with Ile119, Phe120, Asp145, Tyr147, and Tyr150 amino acids (Fig. 4, **video**).

The interactions with Thr147 were found more important and more stable than other interactions since they started uninterrupted after 20 ns. Because the system stability was reached at this time, it can be concluded that the interaction with Thr147 played a key role in the complex stability and the antioxidant activity. On the other hand, Phe120, which is one of the important hydrophobic residues located in helix α5, is not observed in other peroxiredoxin

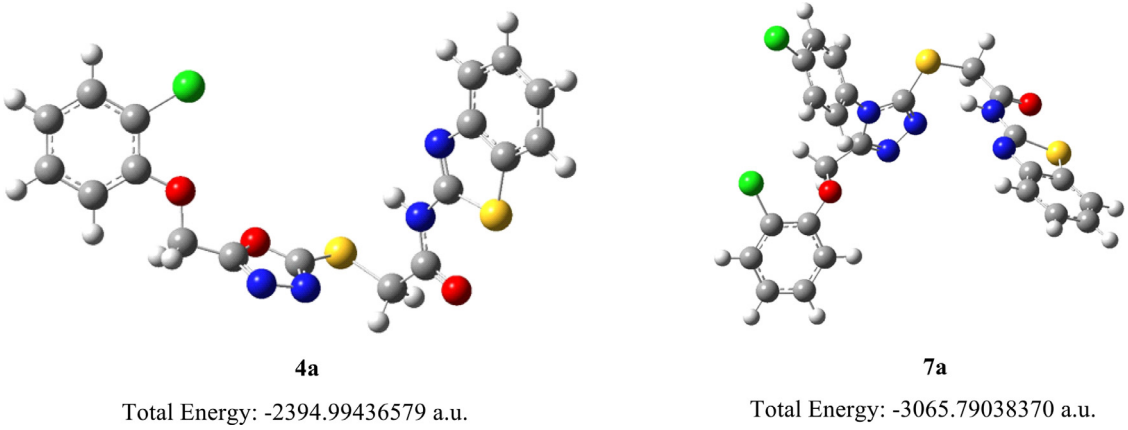

Fig. 5. Optimized molecular structures and total energy values of compounds 4a and 7a.

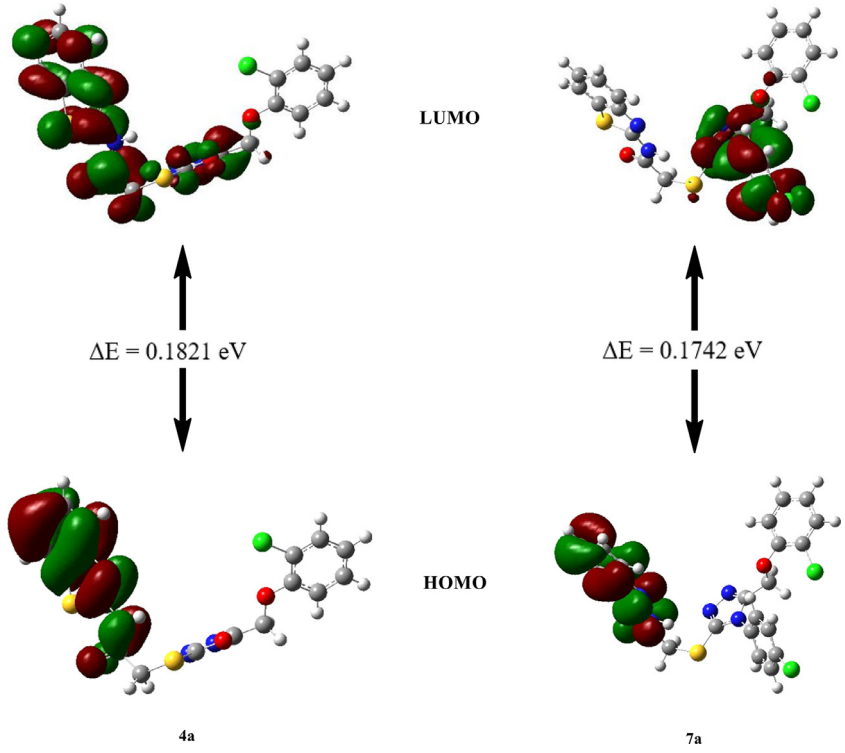

Fig. 6. HOMO-LUMO diagrams of the compounds 4a and 7a.

enzymes [40]. Therefore, it's a unique amino acid for PRDX5 selectivity. Interestingly, an interaction with Phe120 was observable regularly after 23 ns. This implied its role in selectivity, and this interaction also contributed to explaining the structure-activity relationship. However, even if the interaction with Asp145 was stable until 25 ns, it was occasionally interrupted thereafter. Hence, this residue may not have an important role in system stability, but it should not be ignored for its possible contribution to the enzyme activity. Besides, there are significant arginine residues found in the structure of all peroxiredoxins. These arginine amino acids have a pivotal role in interacting with the sulfur atom of Cys47 and seem to be responsible for the positively charged active-site pocket. This positive charge environment allows Cys47 amino acid to lower the pKa of the thiol by stabilizing its ionized state and, thus, increasing the reactivity. Hence, the interaction with arginine residues should possibly result in antioxidant activity. In human PRDX5, the sequence of this arginine amino acid is Arg127 [40]. In our study, we observed that water-mediated and direct H-bonds were formed with Arg127 frequently. Thereby, even if compound **7a** did not interact with Cys47, it bonded Arg127 amino acid and then probably blocked the enzyme activation. This was the answer we were looking for clarifying its mechanism of action. In conclusion, these four amino acids (Phe120, Arg127, Asp145, and Thr147) played important roles in the antioxidant activity of compound **7a**.

2.5. Results of DFT studies

The use of DFT-based global reactivity descriptors to determine the reactivity and site selectivity of various biomolecules has gotten a lot of attention. To investigate the structure, stability, and properties of compounds **4a** and **7a**, we used global reactivity descriptors based on DFT. The three-dimensional structure of the investigated substances can be explained using optimal molecular structures derived from theoretical techniques. When the B3LYP/6–31 G (d,p) basis range was employed to optimize the structures of the most active compounds, **4a** and **7a**, no imaginary frequency

Table 4
Some chemical reactivity parameters of the most active compounds.

Compounds	EHOMO (eV)	ELUMO (eV)	ΔE (eV)	I (eV)	A (eV)	χ (eV)	η (eV)	S (eV−1)	μ (eV)	ω (eV)
4a	−0.2228	−0.0407	0.1821	0.2228	0.0407	0.1317	0.0910	5.4945	−0.1317	0.0953
7a	−0.2207	−0.0465	0.1742	0.2207	0.0465	0.1336	0.0871	5.7405	−0.1336	0.1025

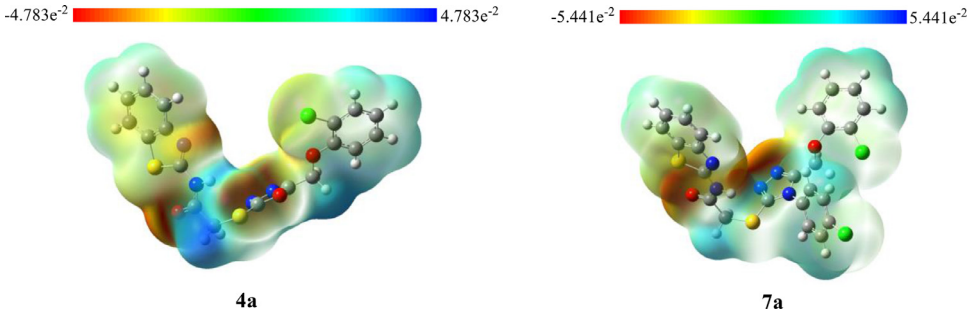

Fig. 7. Molecular electrostatic potential (MEP) surfaces of compounds 4a and 7a.

was observed. Fig. 5 shows the optimized structures of the active compounds **4a** and **7a**.

Frontier molecular orbital analysis of the optimized geometries was performed at the B3LYP/6–31 G (d,p) level. Chemical reactivity, optical polarizability, chemical softness, hardness, and molecular electrical transport characteristics of any chemical system were all determined by the energy difference between HOMO and LUMO [42].

Table 4 shows the energies of frontier molecular orbitals as well as the energy difference between HOMO and LUMO. Negative HOMO and LUMO values were found in compounds **4a** and **7a**, indicating that they were stable (Fig. 6). In addition, the most prominent ionization potential (I) and electron affinity (A) values related to HOMO and LUMO energy are those of compound **7a** with a low I value and a high A value. As a result, the **7a** compound is more nucleophilic than **4a**.

Electronegativity (χ) refers to an atom's proclivity to attract shared electrons (or electron density) to itself. The more electrons are attracted to an atom or a substituent group, the higher the associated electronegativity. Electro-positivity is the polar opposite of electronegativity and measures a molecule's ability to give valence electrons. As we can see, compound **7a** has a higher electronegativity with 0.1336 eV values and a better electrophilic character with 0.1025 eV values than compound **4a**. According to chemical hardness-softness (η, S) values, which are effective in determining intramolecular charge transfer of molecular structures, the compound with a high S and a low η value is **7a**.

The molecular electrostatic potential (MEP) of 3D molecules confirms the charge distribution (positive and negative) and calculates ligand binding and hydrogen bonding with biomolecules [43]. The MEP mapping results of compounds **4a** and **7a** are shown in Fig. 7. The MEP scheme reveals several colors: red represents a partial negative charge because of an electron-rich zone, blue represents a partial positive charge because of an electron-deficient zone, yellow represents a moderately electron-rich zone, and green represents a neutral zone [44]. According to the MEP mapping, the carbonyl moiety, and the oxadiazole and triazole moieties of compounds **4a** and **7a**, respectively, have the highest negative potential.

3. Conclusion

New series of triazole and oxadiazole derivatives were synthesized. The targeted compounds were evaluated for antimicrobial and antioxidant properties. All compounds showed poor antibacterial and antifungal activity, compound **7b** showed half the antimicrobial activity of the standard drug chloramphenicol on *B. subtilis*. Compounds **4a** and **7a** exhibited remarkable antioxidant abilities with IC_{50} values of 2.75 and 2.67 mg/mL whereas ascorbic acid had an IC_{50} value of 0.49 mg/mL. The pharmacokinetic profile of the synthesized compounds was predicted, and it indicated that these molecules are suitable for topical administration to the skin, eyes, ears, or locally in the GIT. The compounds might be considered for drug-target repurposation replacing their targeted antimicrobial activity. The antioxidant abilities of compounds **4a** and **7a** were studied by molecular docking and MDS. The results of the MDS study showed that amino acids Phe120, Arg127, Asp145, and Thr147 play important roles in the antioxidant activity of the tested compounds. DFT calculations results revealed certain chemical characteristics of compounds **4a** and **7a**. Both are very stable compounds, and also have nucleophilic character. Accordingly, 3-chlorophenyl and 4-chlorophenyl containing oxadiazole and triazole skeletons can be synthesized and derivatives containing simple benzothiazole or thiazole can be investigated biologically through similar compounds, in further studies.

4. Materials and methods

4.1. Chemistry

All chemicals used in the syntheses were purchased either from Merck Chemicals (Merck KGaA, Darmstadt, Germany) or Sigma-Aldrich Chemicals (Sigma-Aldrich Corp., St. Louis, MO, USA). The reactions and the purities of the compounds were observed by thin-layer chromatography (TLC) on silica gel 60 F_{254} aluminum sheets obtained from Merck (Darmstadt, Germany). Melting points of the synthesized compounds were recorded by the MP90 digital melting point apparatus (Mettler Toledo, Ohio, USA) and were presented as uncorrected. ^{1}H NMR and ^{13}C NMR spectra were recorded by a Bruker 300 MHz digital FT NMR spectrometer (Bruker Bioscience, Billerica, MA, USA) in DMSO–d_6. In the NMR spectra, splitting patterns were designated as follows: s: singlet; d: doublet; t: triplet; m: multiplet. Coupling constants (J) were reported as Hertz. High-resolution mass spectrometric (HRMS) studies were performed using an LC/MS-IT-TOF system (Shimadzu, Kyoto, Japan).

4.1.1. Synthesis of ethyl 2-(2-chlorophenoxy)acetate (1)

2-Chlorophenol (0.05 mol) and ethyl 2-chloroacetate (0.06 mol, 7.64 mL) were mixed with potassium carbonate (0.075 mol, 10.36 g). The mixture was refluxed in acetone (200 mL) for 24 h.

The solvent was evaporated after TLC approval of the reaction's end. The mixture was filtered, and the obtained residue was washed with water before recrystallization from ethanol.

4.1.2. Synthesis of 2-(2-chlorophenoxy)acetohydrazide (2)

Ethyl 2-(2-chlorophenoxy)acetate (**1**) (0.025 mol, 5.7 g) and hydrazine monohydrate (0.1 mol) were stirred at room temperature in ethanol (100 mL) for 3 h. The addition of hydrazine solved in ethanol into the ethanolic solution of compound **1** was achieved in an ice bath and the mixture was then stirred in RT. After controlling the reaction's endpoint using TLC, stirring was stopped and the mixture was awaited till two phases of solvent and precipitate were formed. The precipitated material was filtered. After drying the product was recrystallized from ethanol.

4.1.3. Synthesis of 5-[(2-chlorophenoxy)methyl]−1,3,4-oxadiazole-2-thiol (3)

2-(2-Chlorophenoxy)acetohydrazide (**2**) (0.016 mol, 3.5 g) was dissolved in ethanol (70 mL) and the solution of cold potassium hydroxide (0.020 mol, 1.14 g) in ethanol (40 mL) was added at room temperature (RT) while the mixture is being stirred. Carbon disulfide (0.48 mol, 2.9 mL) was then added to the mixture at RT, and upon the addition of carbon disulfide a white precipitate was formed immediately which made it difficult to stir. An extra amount of ethanol was added to facilitate the stirring. The mixture was refluxed for 5 h. After completion of the reaction, the solution was cooled and poured into ice water then acidified to pH 4 with dilute HCl. The target product (**3**) was precipitated slowly overnight. It was then obtained by filtration.

4.1.4. General synthesis of N-*(benzothiazol-2-yl)−2-({5-[(2-chlorophenoxy)methyl]−1,3,4-oxadiazol-2-yl}thio)acetamide derivatives (4a–4e)*

N-(Benzothiazol-2-yl)−2-chloroacetamide derivatives (0.001 mol) were reacted separately with 5-[(2-chlorophenoxy)methyl]−1,3,4-oxadiazole-2-thiol (**3**) (0.001 mol, 0.257 g) in acetone (25 mL) with the presence of K_2CO_3 (0.002 mol, 0.27 g). The mixture was allowed to stir overnight at RT. The reaction was monitored via TLC. After the reaction was completed, acetone was removed, and the crude product was washed with water and recrystallized from ethanol.

N-(Benzothiazol-2-yl)−2-({5-[(2-chlorophenoxy)methyl]−1,3,4-oxadiazol-2-yl}thio)acetamide (4a) m. p. 196–197 °C, yield 77%, ^{1}H NMR (300 MHz, DMSO–d_6, ppm) δ 4.45 (s, 2H, S-$\underline{CH_2}$), 5.49 (s, 2H, O–$\underline{CH_2}$), 6.99–7.04 (m, 1H, Ar-H), 7.28–7.35 (m, 3H, Ar-H), 7.41–7.46 (m, 2H, Ar-H), 7.75 (d, J = 8.04 Hz, 1H, Ar-H), 7.97 (d, J = 7.84 Hz, 1H, Ar-H). ^{13}C NMR (75 MHz, DMSO–d_6, ppm) δ 36.42 (S-$\underline{CH_2}$), 60.73 (O–$\underline{CH_2}$), 115.25, 121.03, 122.21, 123.42, 124.03, 126.59, 128.84, 130.68, 131.98, 163.86, 164.98, 166.88. HRMS (*m/z*): $[M + 1]^+$ calculated for $C_{18}H_{13}ClN_4O_3S_2$ 433.0190, found 433.0208.

2-({5-[(2-Chlorophenoxy)methyl]−1,3,4-oxadiazol-2-yl}thio)-N-(6-methylbenzothiazol-2-yl)acetamide (4b) m. p. 290–291 °C, yield 80%, ^{1}H NMR (300 MHz, DMSO–d_6, ppm) δ 2.41 (s, 3H, bth-$\underline{CH_3}$), 4.45 (s, 2H, S-$\underline{CH_2}$), 5.49 (s, 2H, O–$\underline{CH_2}$), 6.99–7.04 (m, 1H, Ar-H), 7.25–7.35 (m, 3H, Ar-H), 7.44 (d, J = 7.88 Hz, 1H, Ar-H), 7.65 (d, J = 8.18 Hz, 1H, Ar-H), 7.77 (s, 1H, Ar-H), 12.73 (brs, 1H, -NH). ^{13}C NMR (75 MHz, DMSO–d_6, ppm) δ 21.47 (bth-$\underline{CH_3}$), 36.12 (S-$\underline{CH_2}$), 60.73 (O–$\underline{CH_2}$), 115.25, 120.81, 121.85, 123.43, 128.02, 128.85, 130.68, 133.70, 153.04, 163.89, 166.48, 178.39. HRMS (*m/z*): $[M + 1]^+$ calculated for $C_{19}H_{15}ClN_4O_3S_2$ 447.0347, found 447.0351.

2-({5-[(2-Chlorophenoxy)methyl]−1,3,4-oxadiazol-2-yl}thio)-N-(6-methoxybenzothiazol-2-yl)acetamide (4c) m. p. 195–196 °C, yield 82%, ^{1}H NMR (300 MHz, DMSO–d_6, ppm) δ 3.80 (s, 3H, bth–O$\underline{CH_3}$), 4.41 (s, 2H, S-$\underline{CH_2}$), 5.49 (s, 2H, O–$\underline{CH_2}$), 7.03 (t, J = 8.99 Hz, 2H, Ar-H), 7.28–7.36 (m, 2H, Ar-H), 7.44 (d, J = 7.32 Hz, 1H, Ar-H), 7.54 (s, 1H, Ar-H), 7.61 (d, J = 8.81 Hz, 1H, Ar-H). ^{13}C NMR (75 MHz, DMSO–d_6, ppm) δ 36.66 (S-$\underline{CH_2}$), 56.02 (bth–O$\underline{CH_3}$), 60.74 (O–$\underline{CH_2}$), 105.09, 115.26, 121.51, 123.43, 128.85, 130.69, 133.37, 153.05, 156.44, 163.79, 166.77. HRMS (*m/z*): $[M + 1]^+$ calculated for $C_{19}H_{15}ClN_4O_4S_2$ 463.0296, found 463.0318.

N-(6-Chlorobenzothiazol-2-yl)−2-({5-[(2-chlorophenoxy)methyl]−1,3,4-oxadiazol-2-yl}thio)acetamide (4d) m. p. 221–222 °C, yield 68%, ^{1}H NMR (300 MHz, DMSO–d_6, ppm) δ 4.47 (s, 2H, S-$\underline{CH_2}$), 5.49 (s, 2H, O–$\underline{CH_2}$), 6.99–7.04 (m, 1H, Ar-H), 7.28–7.35 (m, 2H, Ar-H), 7.45 (t, J = 8.79 Hz, 2H, Ar-H), 7.76 (d, J = 8.64 Hz, 1H, Ar-H), 8.13 (s, 1H, Ar-H), 12.90 (brs, 1H, -NH). ^{13}C NMR (75 MHz, DMSO–d_6, ppm) δ 36.16 (S-$\underline{CH_2}$), 60.72 (O–$\underline{CH_2}$), 115.24, 122.00, 122.15, 122.37, 123.42, 127.03, 128.21, 128.84, 130.68, 133.63, 147.84, 153.03, 159.13, 163.91, 164.86, 166.94. HRMS (*m/z*): $[M + 1]^+$ calculated for $C_{18}H_{12}Cl_2N_4O_3S_2$ 466.9801, found 466.9820.

2-({5-[(2-Chlorophenoxy)methyl]−1,3,4-oxadiazol-2-yl}thio)-*N*-(6-nitrobenzothiazol-2-yl)acetamide (4e) m. p. 203–204 °C, yield 74%, ^{1}H NMR (300 MHz, DMSO–d_6, ppm) δ 4.44 (s, 2H, S-$\underline{CH_2}$), 5.49 (s, 2H, O–$\underline{CH_2}$), 6.99–7.04 (m, 1H, Ar-H), 7.28–7.35 (m, 2H, Ar-H), 7.43 (d, J = 8.60 Hz, 1H, Ar-H), 7.82 (d, J = 8.79 Hz, 1H, Ar-H), 8.24 (d, J = 8.98 Hz, 1H, Ar-H), 8.96 (s, 1H, Ar-H). ^{13}C NMR (75 MHz, DMSO–d_6, ppm) δ 37.20 (S-$\underline{CH_2}$), 60.74 (O–$\underline{CH_2}$), 115.25, 119.19, 120.55, 122.04, 122.15, 123.41, 128.85, 130.67, 132.90, 142.87, 153.04, 154.64, 163.78, 165.17, 168.83. HRMS (*m/z*): $[M + 1]^+$ calculated for $C_{18}H_{12}ClN_5O_5S_2$ 478.0041, found 478.0064.

*4.1.5. Synthesis of 2-[2-(2-chlorophenoxy)acetyl]-*N*-(4-chlorophenyl) hydrazinecarbothioamide (5)*

2-(2-Chlorophenoxy)acetohydrazide (**2**) (0.017 mol, 3.649 g) and 1–chloro-4-isothiocyanatobenzene (0.02 mol, 3.39 g) were refluxed in ethanol (100 mL) for 3 h. TLC was used to observe the reaction's ending. The solvent was evaporated, and the residue was recrystallized from ethanol.

4.1.6. Synthesis of 5-[(2-chlorophenoxy)methyl]−4-(4-chlorophenyl)−4H-1,2,4-triazole-3-thiol (6)

2-[2-(2-Chlorophenoxy)acetyl]-*N*-(4-chlorophenyl) hydrazinecarbothioamide (**5**) (0.014 mol, 5.38 g) was refluxed in 2 M ethanolic potassium hydroxide solution (100 mL). The reaction was monitored via TLC and upon its completion, the mixture was cooled to RT and then poured onto ice water. Next, the mixture was acidified to pH= 3 using a dilute HCl solution. The resulting white precipitate was obtained by filtration.

4.1.7. General synthesis of N-*(benzothiazol-2-yl)−2-({5-[(2-chlorophenoxy)methyl]−4-(4-chlorophenyl)−4*H-*1,2,4-triazol-3-yl}thio)acetamide derivatives (7a–7e)*

5-[(2-Chlorophenoxy)methyl]−4-(4-chlorophenyl)−4*H*-1,2,4-triazole-3-thiol (**6**) (0.001 mol, 0.37 g) and equivalent amounts (0.001 mol) *N*-(benzothiazol-2-yl)−2-chloroacetamide derivatives were reacted in the presence of potassium carbonate (0.001 mol, 0.14 g) in 50 mL acetone. From the reaction mixture, the solvent was evaporated after the reaction completion and the residue was washed with water to yield the final product. All final compounds were recrystallized from ethanol.

N-(Benzothiazol-2-yl)−2-({5-[(2-chlorophenoxy)methyl]−4-(4-chlorophenyl)−4H-1,2,4-triazol-3-yl}thio)acetamide (7a) m. p. 249–250 °C, yield 86%, ^{1}H NMR (300 MHz, DMSO–d_6, ppm) δ 4.31 (s, 2H, S-$\underline{CH_2}$), 5.22 (s, 2H, O–$\underline{CH_2}$), 6.95 (t, J = 6.97 Hz, 1H, Ar-H), 7.20 (t, J = 6.59 Hz, 1H, Ar-H), 7.24–7.29 (m, 1H, Ar-H), 7.31–7.38 (m, 2H, Ar-H), 7.45 (t, J = 6.71 Hz, 1H, Ar-H), 7.57–7.65 (m, 4H, Ar-H), 7.76 (d, J = 7.90 Hz, 1H, Ar-H), 7.98 (d, J = 7.30 Hz, 1H, Ar-H), 12.68 (brs, 1H, -NH). ^{13}C NMR (75 MHz, DMSO–d_6, ppm) δ 35.89 (S-$\underline{CH_2}$), 60.41 (O–$\underline{CH_2}$), 114.47, 118.86, 120.66, 121.49, 121.78, 122.50, 123.68, 126.20, 128.22, 129.02, 129.49, 129.84,

130.05, 131.30, 131.48, 134.94, 151.46, 152.50, 157.83, 166.94. HRMS (*m/z*): $[M + 1]^+$ calculated for $C_{24}H_{17}Cl_2N_5O_2S_0$ 542.0273, found 542.0290.

2-({5-[(2-Chlorophenoxy)methyl]−4-(4-chlorophenyl)−4*H*-1,2,4-triazol-3-yl}thio)-*N*-(6-methylbenzothiazol-2-yl)acetamide (7b) m. p. 271–272 °C, yield 89%, ^{1}H NMR (300 MHz, DMSO–d_6, ppm) δ 2.41 (s, 3H, bth-$\underline{CH_3}$), 4.30 (s, 2H, S-$\underline{CH_2}$), 5.22 (s, 2H, O–$\underline{CH_2}$), 6.95 (t, J = 6.94 Hz, 1H, Ar-H), 7.21 (t, J = 6.58 Hz, 1H, Ar-H), 7.26 (d, J = 8.85 Hz, 2H, Ar-H), 7.35–7.43 (m, 1H, Ar-H), 7.61 (d, J = 5.20 Hz, 3H, Ar-H), 7.63–7.66 (m, 2H, Ar-H), 7.77 (s, 1H, Ar-H), 12.63 (brs, 1H, -NH). ^{13}C NMR (75 MHz, DMSO–d_6, ppm) δ 21.45 (bth-$\underline{CH_3}$), 36.25 (S-$\underline{CH_2}$), 60.82 (O–$\underline{CH_2}$), 114.86, 120.76, 121.89, 122.94, 127.99, 128.67, 129.46, 129.94, 130.30, 130.50, 131.73, 132.04, 133.61, 135.38, 151.89, 151.95, 152.93, 157.36, 167.23. HRMS (*m/z*): $[M + 1]^+$ calculated for $C_{25}H_{19}Cl_2N_5O_2S_2$ 556.0430, found 556.0452.

2-({5-[(2-Chlorophenoxy)methyl]−4-(4-chlorophenyl)−4*H*-1,2,4-triazol-3-yl}thio)-*N*-(6-methoxybenzothiazol-2-yl)acetamide (7c) m. p. 241–242 °C, yield 91%, ^{1}H NMR (300 MHz, DMSO–d_6, ppm) δ 3.80 (s, 3H, bth–O$\underline{CH_3}$), 4.29 (s, 2H, S-$\underline{CH_2}$), 5.23 (s, 2H, O–$\underline{CH_2}$), 6.95 (t, J = 6.13 Hz, 1H, Ar-H), 7.04 (d, J = 8.84 Hz, 1H, Ar-H), 7.18–7.28 (m, 2H, Ar-H), 7.35–7.43 (m, 1H, Ar-H), 7.58 (s, 1H, Ar-H), 7.61 (d, J = 5.52 Hz, 3H, Ar-H), 7.63–7.67 (m, 2H, Ar-H), 12.58 (brs, 1H, -NH). ^{13}C NMR (75 MHz, DMSO–d_6, ppm) δ 36.21 (S-$\underline{CH_2}$), 56.09 (bth–O$\underline{CH_3}$), 60.82 (O–$\underline{CH_2}$), 105.15, 114.87, 115.48, 121.74, 121.90, 122.94, 128.68, 129.46, 130.31, 130.50, 131.73, 133.23, 135.39, 143.03, 151.89, 151.96, 152.93, 156.18, 156.64, 167.06. HRMS (*m/z*): $[M + 1]^+$ calculated for $C_{25}H_{19}Cl_2N_5O_3S_2$ 572.0379, found 572.0375.

N-(6-Chlorobenzothiazol-2-yl)−2-({5-[(2-chlorophenoxy)methyl]−4-(4-chlorophenyl)−4*H*-1,2,4-triazol-3-yl}thio)acetamide (7d) m. p. 230–231 °C, yield 78%, ^{1}H NMR (300 MHz, DMSO–d_6, ppm) δ 4.27 (s, 2H, S-$\underline{CH_2}$), 5.22 (s, 2H, O–$\underline{CH_2}$), 6.95 (t, J = 6.96 Hz, 1H, Ar-H), 7.18–7.28 (m, 2H, Ar-H), 7.36 (d, J = 7.80 Hz, 1H, Ar-H), 7.42 (d, J = 8.63 Hz, 1H, Ar-H), 7.57–7.65 (m, 4H, Ar-H), 7.69 (d, J = 8.67 Hz, 1H, Ar-H), 8.07 (s, 1H, Ar-H). ^{13}C NMR (75 MHz, DMSO–d_6, ppm) δ 36.97 (S-$\underline{CH_2}$), 60.83 (O–$\underline{CH_2}$), 114.87, 121.77, 121.91, 121.97, 122.93, 126.66, 127.60, 128.68, 129.47, 130.29, 130.50, 131.78, 133.85, 135.36, 148.17, 151.79, 152.23, 152.94, 168.32. HRMS (*m/z*): $[M + 1]^+$ calculated for $C_{24}H_{16}Cl_3N_5O_2S_2$ 575.9884, found 575.9898.

2-({5-[(2-Chlorophenoxy)methyl]−4-(4-chlorophenyl)−4*H*-1,2,4-triazol-3-yl}thio)-*N*-(6-fluorobenzothiazol-2-yl)acetamide (7e) m. p. 243–244 °C, yield 84%, ^{1}H NMR (300 MHz, DMSO–d_6, ppm) δ 4.30 (s, 2H, S-$\underline{CH_2}$), 5.22 (s, 2H, O–$\underline{CH_2}$), 6.95 (t, J = 6.94 Hz, 1H, Ar-H), 7.18–7.27 (m, 2H, Ar-H), 7.29–7.38 (m, 2H, Ar-H), 7.57–7.65 (m, 4H, Ar-H), 7.74–7.79 (m, 1H, Ar-H), 7.89 (d, J = 8.59 Hz, 1H, Ar-H), 12.74 (brs, 1H, -NH). ^{13}C NMR (75 MHz, DMSO–d_6, ppm) δ 36.32 (S-$\underline{CH_2}$), 60.83 (O–$\underline{CH_2}$), 108.50, 108.85, 114.58, 114.87, 121.90, 122.13, 122.25, 122.94, 128.67, 129.46, 130.30, 130.50, 131.73, 135.39, 145.71, 151.89, 157.53, 158.47, 160.70, 167.59. HRMS (*m/z*): $[M + 1]^+$ calculated for $C_{24}H_{16}Cl_2FN_5O_2S_2$ 560.0179, found 560.0171.

4.2. Pharmacokinetic parameters

Some physicochemical and pharmacokinetic properties of the final compounds were predicted via SwissADME which is a web-based software [45]. H-bond acceptor (HBA, recommended by Lipinski's Rule of Five (RoF) to be ≤10 [46,47], H-bond donor (HBD recommended by Lipinski's Rule of Five (RoF) to be ≤5), topologic polar surface area (TPSA, recommended by Veber et al. to be ≤140 Å^2 [48], lipophilicity descriptor (octanol/water partition, consensus Log Po/w where the recommended value is between −0.7 and 5) [45], water solubility (Log S, recommended between −6.5 and 5 [45], gastrointestinal absorption (GIA), skin permeation (Log Kp, cm/s), violation number to the Rule of Five (RoF (V), synthetic accessibility from very easy to very difficult 1 to 10 (SA) were calculated *in silico*.

4.3. Biology

4.3.1. Antimicrobial activity

The antimicrobial activity of the compounds was tested on microorganisms including *E. coli* (ATCC 25922), *Bacillus cereus* (ATCC 10876), *Bacillus subtilis* (NRRL NRS-744), *Staphylococcus aureus* (ATCC 6538), *Salmonella typhimurium* (ATCC 14028), and *Micrococcus luteus* (NRRL B-4375) as bacteria; *Candida parapsilosis* (ATCC 22019), *Candida albicans* (ATCC 90028), *Candida glabrata* (ATCC 90030), and *Candida krusei* (ATCC 6258) as Yeasts; *Aspergillus niger* (ATCC 9807), *Aspergillus flavus* (ATCC 9807), *Aspergillus parasiticus* (NRRL 465), *Aspergillus fumigatus* (NRRL 113), *Penicillium notatum* (clinical isolate), and *Penicillium chryrsogenum* (ATCC 10106) as filamentous fungi. Mueller-Hinton agar plates were used to maintain bacterial cultures. Potato dextrose (PD) agar and Sabourad dextrose (SD) agar were used for the maintenance of fungal cultures. Test bacteria were acquired from bacterial cultures the incubation of which was performed for 24 h at 37 °C on Mueller-Hinton agar substrate and the dilution of which was performed in accordance with the 0.5 McFarland standard to about 10^8 CFU/mL. Fresh mature cultures at the age of 3 to 7 days growing at 30 °C on a PD agar substrate were used for the preparation of fungal spore suspensions. Sterile 0.1% Tween 80 was used for the rinsing of the spores and their further dilution to about 10^6 CFU/mL was performed by the procedural recommendations of CLSI [49]. The minimum inhibitory concentration (MIC) of the substances was determined by a serial dilution technique using 96-well microtitre plates. A stock solution of 80 mg of each of the substances in 10 ml DMSO (20%) was prepared and subsequently diluted two-fold with Mueller-Hinton broth ten times in the case of bacterial cultures and SD broth was utilized in the case of fungal cultures. Several dilutions, the concentrations of which varied between 8 mg/ml and 15.625 μg/mL. 100 μL from bacteria, yeasts, and fungal spore solutions and dilutions were transferred into microtitration plates and incubated for 24–48 h at 35–37 °C for bacteria/yeasts and 25 °C for filamentous fungi. One of the positive controls contained 100 μL of microorganism solution plus 20% DMSO solution in a well and another one had 100 μL of microorganism solution plus 100 μL Mueller-Hinton broth in a well. The third control was chloramphenicol for bacterium and ketoconazole for fungi. Negative controls contained only dilute solutions without microorganisms. Positive and negative results were evaluated according to turbidity that occurred after 24–48 h in the test samples compared to the controls. The lowest concentrations giving no visible growth for each microorganism were defined as MIC. The determination of the minimal inhibitory concentration was performed using resazurin, which indicates oxidation–reduction and is employed for the assessment of microbial growth. Resazurin represents a non-fluorescent dye of blue color which turns pink and fluorescent in the case of reduction to resazurin with oxidoreductases inside viable cells. The minimal inhibitory concentration (MIC) for the microorganism examined at the determined concentration was described as the boundary dilution with no altering color of resazurin [50].

4.3.2. Antioxidant activity by scavenging DPPH radicals

The antioxidant activity of the synthesized substances was measured based on the ability to capture the free radical by using 1, 1-diphenyl-2-picryl-hydrazyl (DPPH) [51]. First, 0.6 mM of DPPH in a methanol solution was prepared by dissolving 0.0238 g of DPPH into 100 mL of methanol. 10 mL of the solution was diluted to 100 mL with methanol to prepare the final stock solution

(0.06 mM) of DPPH, which was stored in a dark environment at room temperature. Secondly, each substance was diluted between 20 and 0.0.039 mg/mL with DMSO by applying a 1:1 serial dilution method. A volume of 250 µL of each concentration (20, 10, 5, 2.5, 1.25, 0.625, 0.313, 0.156, 0.078, and 0.039 mg/mL) of the substances was mixed with 750 µL of 0.06 mM methanolic solution of DPPH and then incubated in darkness at room temperature for 30 minutes followed by measuring the absorbance at 520 nm using a UV spectrophotometer. The free radical scavenging ability of the extract solutions is indicated as% inhibition of DPPH absorbance. The calculation of the remaining DPPH was done as given in the following equation.

$$\text{DPPH scavenging effect (I) (\% Inhibition)} = [(A_0 - A_1)\ /A_{0|}\ \text{x}\ 100 \quad (1)$$

A_0 = The absorbance of the control sample.
A_1 = The absorbance in the existence of all samples or references.

By using these values, the sample concentration (IC_{50}) values were calculated when half of the DPPH free radical was scavenged. Values were compared with the antioxidant ascorbic acid (1 mg/mL) [52].

4.4. Methods for in silico studies

4.4.1. Molecular docking studies

Molecular docking studies were performed using an *in silico* procedure to define the binding modes of the active compounds in the active regions of enzymes X-ray crystal structure of peroxiredoxin 5 enzyme (PRDX5, PDB ID: 1HD2) to understand the antioxidant activity. X-ray crystal structure of peroxiredoxin 5 was retrieved from the Protein Data Bank server (www.pdb.org, accessed 07 December 2022). Schrödinger Maestro [53] interface was used for the molecular docking study and the enzyme crystals were processed using the Protein Preparation Wizard protocol of the Schrödinger Suite 2020. Active compounds were prepared using the LigPrep module [54] to correctly assign the protonation states as well as the atom types. Bond orders were assigned, and hydrogen atoms were added to the structures. The grid generation was formed using the Glide module [55], and docking runs were performed in standard precision docking mode (SP).

4.4.2. Molecular dynamics simulation (MDS) studies

MDS has been considered an important computational tool for evaluating the time-dependent stability of the ligand-receptor complex. In this study, MDS for 50 ns was carried out to ensure the stability of the identified hits from the docking results. We performed Desmond application [56] using the standard force field (OPLS3e) of the Schrodinger Suite with a transferable intermolecular potential with 3 points (TIP3P) water model followed by energy minimization of the complex. The neutralization of the system was achieved using Na^+ and Cl^- ions and 150 mM NaCl was added to the dynamic condition. The molecular dynamics simulation was performed following the completion of the system setup. The radius of gyration (Rg), root mean square fluctuation (RMSF), and root mean square deviation (RMSD) values were calculated by the Desmond application.

4.5. DFT studies

Theoretical approaches for our active compounds were performed using molecular visualization programs: the Gaussian 09 W package [57] and GaussView 5.0 [58]. The electronic characteristics of the active compounds (**4a** and **7a**) were investigated using density functional theory (DFT) at the B3LYP/6-31G (d, p) level using previously published procedures [59,60].

Declaration of Competing Interest

The authors declare that they have no known competing financial interests or personal relationships that could have appeared to influence the work reported in this paper.

CRediT authorship contribution statement

Sam Dawbaa: Conceptualization, Methodology, Software, Validation, Formal analysis, Investigation, Data curation, Writing – original draft, Writing – review & editing, Visualization. **Demokrat Nuha:** Software, Formal analysis, Visualization. **Asaf Evrim Evren:** Software, Formal analysis, Visualization. **Meral Yilmaz Cankiliç:** Investigation, Resources. **Leyla Yurttaş:** Conceptualization, Methodology, Validation, Resources, Data curation, Writing – original draft, Writing – review & editing, Project administration, Funding acquisition, Supervision. **Gülhan Turan:** Conceptualization, Methodology, Resources, Project administration, Funding acquisition.

Data Availability

The data are available in the supplemental data file

Acknowledgements

The authors present their gratitude to DOPNA laboratory and Anadolu University.

Supplementary materials

Supplementary material associated with this article can be found, in the online version, at doi:10.1016/j.molstruc.2023.135213.

References

[1] M. Billah, A. Wahab, M. Islam, M.M. Alam, Antimicrobial resistance crisis and combating approaches, J Med 20 (2019) 38–45, doi:10.3329/jom.v20i1.38842.
[2] J. Davies, Inactivation of antibiotics and the dissemination of resistance genes, Science 264 (1994) 375–382.
[3] X. Zhao, H. Su, W. Xu, X. Hu, Y. Xu, G. Wen, Y. Cao, Removal of antibiotic resistance genes and inactivation of antibiotic-resistant bacteria by oxidative treatments, Sci. Total Environ. 778 (2021) 146348.
[4] M. Unemo, J. Ahlstrand, L. Sánchez-Busó, M. Day, D. Aanensen, D. Golparian, S. Jacobsson, M.J. Cole, High susceptibility to zoliflodacin and conserved target (GyrB) for zoliflodacin among 1209 consecutive clinical Neisseria gonorrhoeae isolates from 25 European countries, 2018, J. Antimicrob. Chemother. 76 (2021) 1221–1228.
[5] H. Cho, R. Misra, Mutational activation of antibiotic-resistant mechanisms in the absence of major drug efflux systems of Escherichia coli, J. Bacteriol. 203 (2021) e00109–e00121.
[6] N.S. Sundaramoorthy, S. Nagarajan, Can nanoparticles help in the battle against drug-resistant bacterial infections in “Post-Antibiotic Era”? in: Antimicrobial Resistance, Springer, 2022, pp. 175–213.
[7] N. Goel, S.W. Fatima, S. Kumar, R. Sinha, S.K. Khare, Antimicrobial resistance in biofilms: exploring marine actinobacteria as a potential source of antibiotics and biofilm inhibitors, Biotechnol. Rep. 30 (2021) e00613.
[8] D.A. Stevens, B.J. Kullberg, E. Brummer, A. Casadevall, M.G. Netea, A.M. Sugar, Combined treatment: antifungal drugs with antibodies, cytokines or drugs, Med Mycol 38 (2000) 305–315, doi:10.1080/mmy.38.s1.305.315.
[9] J.t. Riddell, G.M. Comer, C.A. Kauffman, Treatment of endogenous fungal endophthalmitis: focus on new antifungal agents, Clin. Infect. Dis. 52 (2011) 648–653, doi:10.1093/cid/ciq204.
[10] E.S.D. Ashley, R. Lewis, J.S. Lewis, C. Martin, D. Andes, Pharmacology of systemic antifungal agents, Clin. Infect. Dis. 43 (2006) S28–S39, doi:10.1086/504492.
[11] M.D. Johnson, C. MacDougall, L. Ostrosky-Zeichner, J.R. Perfect, J.H. Rex, Combination antifungal therapy, Antimicrob. Agents Chemother. 48 (2004) 693–715, doi:10.1128/AAC.48.3.693-715.2004.
[12] Z. Luo, H. Cui, J. Guo, J. Yao, X. Fang, F. Yan, B. Wang, H. Mao, Poly (ionic liquid)/Ce-based antimicrobial nanofibrous membrane for blocking drug-resistance dissemination from MRSA-infected wounds, Adv Funct Mater 31 (2021) 2100336.

[13] R.C.D. Furniss, N. Kaderabkova, D. Barker, P. Bernal, E. Maslova, A.A. Antwi, H.E. McNeil, H.L. Pugh, L. Dortet, J.M. Blair, Breaking antimicrobial resistance by disrupting extracytoplasmic protein folding, Elife 11 (2022) e57974.
[14] X. Fan, F. Yang, C. Nie, L. Ma, C. Cheng, R. Haag, Biocatalytic nanomaterials: a new pathway for bacterial disinfection, Adv. Mater. 33 (2021) 2100637.
[15] G. Casillas-Vargas, C. Ocasio-Malavé, S. Medina, C. Morales-Guzmán, R.G. Del Valle, N.M. Carballeira, D.J. Sanabria-Ríos, Antibacterial fatty acids: an update of possible mechanisms of action and implications in the development of the next-generation of antibacterial agents, Prog Lipid Res 82 (2021) 101093.
[16] S. Dawbaa, A.E. Evren, Z. Cantürk, L. Yurttaş, Synthesis of new thiazole derivatives and evaluation of their antimicrobial and cytotoxic activities, Phosphorus Sulfur Silicon Relat. Elem. 196 (2021) 1093–1102, doi:10.1080/10426507.2021.1972299.
[17] D. Nuha, A.E. Evren, M. Yılmaz Cankılıç, L. Yurttaş, Design and synthesis of novel 2,4,5-thiazole derivatives as 6-APA mimics and antimicrobial activity evaluation, Phosphorus Sulfur Silicon Relat. Elem. 196 (2021) 954–960, doi:10.1080/10426507.2021.1946537.
[18] L. Yurttaş, A. Kubilay, A.E. Evren, İ. Kısacık, H.Karaca Gençer, Synthesis of some novel 3,4,5-trisubstituted triazole derivatives bearing quinoline ring and evaluation of their antimicrobial activity, Phosphorus Sulfur Silicon Relat. Elem. 195 (2020) 767–773, doi:10.1080/10426507.2020.1756808.
[19] U.A. Cevik, B.N. Saglik, Y. Ozkay, Z. Canturk, J. Bueno, F. Demirci, A.S. Koparal, Synthesis of new fluoro-benzimidazole derivatives as an approach towards the discovery of novel intestinal antiseptic drug candidates, Curr Pharm Des 23 (2017) 2276–2286, doi:10.2174/1381612822666161201150131.
[20] G. Sulis, S. Sayood, S. Gandra, Antimicrobial resistance in low-and middle-income countries: current status and future directions, Expert Rev. Anti-Infect. Ther. 20 (2022) 147–160.
[21] J. Cama, R. Leszczynski, P. Tang, A. Khalid, V. Lok, C. Dowson, A. Ebata, To push or to pull? In a post-COVID world, supporting and incentivizing antimicrobial drug development must become a governmental priority, ACS Infect. Dis. 7 (2021) 2029–2042.
[22] R. Kundu, P. Payal, Antimicrobial hydrogels: promising soft biomaterials, ChemistrySelect 5 (2020) 14800–14810.
[23] Y. Nural, S. Ozdemir, M.S. Yalcin, B. Demir, H. Atabey, Z. Seferoglu, A. Ece, New bis-and tetrakis-1, 2, 3-triazole derivatives: synthesis, DNA cleavage, molecular docking, antimicrobial, antioxidant activity and acid dissociation constants, Bioorg. Med. Chem. Lett. 55 (2022) 128453.
[24] İ. Şahin, F.B. Özgeriş, M. Köse, E. Bakan, F. Tümer, Synthesis, characterization, and antioxidant and anticancer activity of 1, 4-disubstituted 1, 2, 3-triazoles, J. Mol. Struct. 1232 (2021) 130042.
[25] S.A.R. Naqvi, S. Nadeem, S. Komal, S.A.A. Naqvi, M.S. Mubarik, S.Y. Qureshi, S. Ahmad, A. Abbas, M. Zahid, S.S. Raza, Antioxidants: natural antibiotics, Antioxidants, IntechOpen, 2019.
[26] L. Wu, Y. Zhou, M.N. Abbas, S. Kausar, Q. Chen, C.X. Jiang, L.S. Dai, Molecular structure and functional characterization of the peroxiredoxin 5 in Procambarus clarkii following LPS and Poly I:C challenge, Fish Shellfish Immunol. 71 (2017) 28–34, doi:10.1016/j.fsi.2017.09.072.
[27] M. Incerti, P. Vicini, A. Geronikaki, P. Eleftheriou, A. Tsagkadouras, P. Zoumpoulakis, C. Fotakis, A. Ciric, J. Glamoclija, M. Sokovic, New N-(2-phenyl-4-oxo-1,3-thiazolidin-3-yl)-1,2-benzothiazole-3-carboxamides and acetamides as antimicrobial agents, Medchemcomm 8 (2017) 2142–2154, doi:10.1039/c7md00334j.
[28] S. Saeed, N. Rashid, P.G. Jones, M. Ali, R. Hussain, Synthesis, characterization and biological evaluation of some thiourea derivatives bearing benzothiazole moiety as potential antimicrobial and anticancer agents, Eur. J. Med. Chem. 45 (2010) 1323–1331, doi:10.1016/j.ejmech.2009.12.016.
[29] S. Bondock, W. Fadaly, M.A. Metwally, Synthesis and antimicrobial activity of some new thiazole, thiophene and pyrazole derivatives containing benzothiazole moiety, Eur. J. Med. Chem. 45 (2010) 3692–3701, doi:10.1016/j.ejmech.2010.05.018.
[30] L. Yurttaş, Y. Özkay, M. Duran, G. Turan-Zitouni, A. Özdemir, Z. Cantürk, K. Küçükoğlu, Z.A. Kaplancıklı, Synthesis and antimicrobial activity evaluation of new dithiocarbamate derivatives bearing thiazole/benzothiazole rings, Phosphorus Sulfur Silicon Relat. Elem. 191 (2016) 1166–1173, doi:10.1080/10426507.2016.1150277.
[31] R.F.A. Gomes, V.M.S. Isca, K. Andrade, P. Rijo, C.A.M. Afonso, Functionalized cyclopentenones and an oxime ether as antimicrobial agents, ChemMedChem 16 (2021) 2781–2785, doi:10.1002/cmdc.202100369.
[32] M. Martínez-Serrano, M. Gerónimo-Pardo, Á. Martínez-Monsalve, M.D. Crespo-Sánchez, Antibacterial effect of sevoflurane and isoflurane, Rev. Esp. Quimioter. 30 (2017) 84–89.
[33] A.M. Lone, M.A. Rather, M.A. Bhat, Z.S. Bhat, I.Q. Tantry, P. Prakash, Synthesis and in vitro evaluation of 2-(((2-ether)amino)methylene)-dimedone derivatives as potential antimicrobial agents, Microb. Pathog. 114 (2018) 431–435, doi:10.1016/j.micpath.2017.12.022.
[34] G. Sui, D. Xu, T. Luo, H. Guo, G. Sheng, D. Yin, L. Ren, H. Hao, W. Zhou, Design, synthesis and antifungal activity of amide and imine derivatives containing a kakuol moiety, Bioorg. Med. Chem. Lett. 30 (2020) 126774, doi:10.1016/j.bmcl.2019.126774.
[35] M. Wang, Y. Du, C. Ling, Z. Yang, B. Jiang, H. Duan, J. An, X. Li, X. Yang, Design, synthesis and antifungal/anti-oomycete activity of pyrazolyl oxime ethers as novel potential succinate dehydrogenase inhibitors, Pest Manag. Sci. 77 (2021) 3910–3920, doi:10.1002/ps.6418.
[36] S. Bitla, A.A. Gayatri, M.R. Puchakayala, V. Kumar Bhukya, J. Vannada, R. Dhanavath, B. Kuthati, D. Kothula, S.R. Sagurthi, K.R. Atcha, Design and synthesis, biological evaluation of bis-(1,2,3- and 1,2,4)-triazole derivatives as potential antimicrobial and antifungal agents, Bioorg. Med. Chem. Lett. 41 (2021) 128004, doi:10.1016/j.bmcl.2021.128004.
[37] T. Glomb, P. Swiatek, Antimicrobial activity of 1,3,4-oxadiazole derivatives, Int J Mol Sci 22 (2021), doi:10.3390/ijms22136979.
[38] 2-Amino-4-methylthiazole, Org. Synth. 19 (1939) 10, doi:10.15227/orgsyn.019.0010.
[39] C.A. Lipinski, F. Lombardo, B.W. Dominy, P.J. Feeney, Experimental and computational approaches to estimate solubility and permeability in drug discovery and development settings 1PII of original article: S0169-409X(96)00423-1. The article was originally published in advanced Drug Delivery Reviews 23 (1997) 3–25. 1, Adv Drug Deliv Rev 46 (2001) 3–26, doi:10.1016/s0169-409x(00)00129-0.
[40] J.P. Declercq, C. Evrard, A. Clippe, D.V. Stricht, A. Bernard, B. Knoops, Crystal structure of human peroxiredoxin 5, a novel type of mammalian peroxiredoxin at 1.5 A resolution, J Mol Biol 311 (2001) 751–759, doi:10.1006/jmbi.2001.4853.
[41] E.D. Dincel, E. Gursoy, T. Yilmaz-Ozden, N. Ulusoy-Guzeldemirci, Antioxidant activity of novel imidazo[2,1-b]thiazole derivatives: design, synthesis, biological evaluation, molecular docking study and in silico ADME prediction, Bioorg Chem 103 (2020) 104220, doi:10.1016/j.bioorg.2020.104220.
[42] C.B.P. Kumar, M.S. Raghu, K.N.N. Prasad, S. Chandrasekhar, B.K. Jayanna, F.A. Alharthi, M.K. Prashanth, K.Y. Kumar, Investigation of biological activity of 2,3-disubstituted quinazolin-4(1H)-ones against Mycobacterium tuberculosis and DNA via docking, spectroscopy and DFT studies, New J. Chem. 45 (2021) 403–414, doi:10.1039/d0nj03800h.
[43] P. Politzer, J.S. Murray, The fundamental nature and role of the electrostatic potential in atoms and molecules, Theor. Chem. Acc. 108 (2002) 134–142, doi:10.1007/s00214-002-0363-9.
[44] F.J. Luque, M. Orozco, P.K. Bhadane, S.R. Gadre, SCRF calculation of the effect of water on the topology of the molecular electrostatic potential, J. Phys. Chem. 97 (2002) 9380–9384, doi:10.1021/j100139a021.
[45] A. Daina, O. Michielin, V. Zoete, SwissADME: a free web tool to evaluate pharmacokinetics, drug-likeness and medicinal chemistry friendliness of small molecules, Sci. Rep. 7 (2017) 42717, doi:10.1038/srep42717.
[46] C.A. Lipinski, F. Lombardo, B.W. Dominy, P.J. Feeney, Experimental and computational approaches to estimate solubility and permeability in drug discovery and development settings, Adv. Drug Deliv. Rev. 23 (1997) 3–25, doi:10.1016/s0169-409x(96)00423-1.
[47] C.A. Lipinski, Lead- and drug-like compounds: the rule-of-five revolution, Drug Discov. Today Technol. 1 (2004) 337–341, doi:10.1016/j.ddtec.2004.11.007.
[48] D.F. Veber, S.R. Johnson, H.Y. Cheng, B.R. Smith, K.W. Ward, K.D. Kopple, Molecular properties that influence the oral bioavailability of drug candidates, J. Med. Chem. 45 (2002) 2615–2623, doi:10.1021/jm020017n.
[49] CLSIMethods For Dilution Antimicrobial Susceptibility Tests For Bacteria That Grow Aerobically; Approved Standard—Ninth edition. CLSI Document M07-A9, Clinical and Laboratory Standards Institute, Wayne, Pennsylvania, USA, 2012.
[50] S.D. Sarker, L. Nahar, Y. Kumarasamy, Microtitre plate-based antibacterial assay incorporating resazurin as an indicator of cell growth, and its application in the in vitro antibacterial screening of phytochemicals, Methods 42 (2007) 321–324, doi:10.1016/j.ymeth.2007.01.006.
[51] W. Brand-Williams, M.E. Cuvelier, C. Berset, Use of a free radical method to evaluate antioxidant activity, LWT - Food Sci. Technol. 28 (1995) 25–30, doi:10.1016/s0023-6438(95)80008-5.
[52] C. Sanchez-Moreno, Review: methods used to evaluate the free radical scavenging activity in foods and biological systems, Food Sci. Technol. Int. 8 (2002) 121–137, doi:10.1106/108201302026770.
[53] Schrödinger Release 2020-3, Maestro, Schrödinger, LLC, New York, NY, USA, 2020.
[54] Schrödinger release. 2020-3: LigPrep 2020, Schrödinger, LLC, New York, NY, USA, 2020.
[55] Schrödinger Release 2020-3, Glide, Schrödinger, LLC, New York, NY, USA, 2020.
[56] Schrödinger Release 2020-3, Desmond, Schrödinger, LLC, New York, NY, USA, 2020.
[57] M. Frisch, G. Trucks, H. Schlegel, G. Scuseria, M. Robb, J. Cheeseman, G. Scalmani, V. Barone, B. Mennucci, G. Petersson, in: Gaussian09, Revision A, Wallingford CT Inc., 2009, pp. 150–166.
[58] R. Dennington, T. Keith, J. Millam, GaussView, version 5, 2009.
[59] D. Nuha, A.E. Evren, Z.S. Ciyanci, H.E. Temel, G. Akalin Ciftci, L. Yurttas, Synthesis, density functional theory calculation, molecular docking studies, and evaluation of novel 5-nitrothiophene derivatives for anticancer activity, Arch. Pharm. (2022) e2200105, doi:10.1002/ardp.202200105.
[60] D. Nuha, H. Berber, A.Ç. Karaburun, A DFT Study of the chemical reactivity properties of Alzheimer's disease medications, SSRN Electron. J. (2022), doi:10.2139/ssrn.4113642.